

Article

Microstructural Evolution and Short-Term Creep Rupture of the Simulated HAZ in T92 Steel Normalized at Different Temperatures

Tai-Jung Wu ^{1,2}, Chien-Chun Liao ¹, Tai-Cheng Chen ² , Ren-Kae Shiue ³  and Leu-Wen Tsay ^{1,*} 

¹ Department of Optoelectronics and Materials Technology, National Taiwan Ocean University, Keelung 20224, Taiwan; gordon@iner.gov.tw (T.-J.W.); jackyliao30@gmail.com (C.-C.L.)

² Nuclear Fuels and Materials Division, Institute of Nuclear Energy Research, Taoyuan 32546, Taiwan; tcchen@iner.gov.tw

³ Department of Materials Science and Engineering, National Taiwan University, Taipei 10617, Taiwan; rkshiue@ntu.edu.tw

* Correspondence: b0186@mail.ntou.edu.tw; Tel.: +886-2-24622192 (ext. 6405)

Received: 18 October 2019; Accepted: 3 December 2019; Published: 5 December 2019



Abstract: T92 steel tubes have been widely applied in advanced supercritical boilers to replace Gr.91 tubes. Simulated samples with microstructures similar to those present in the heat-affected zone (HAZ) of a T92 steel weld were subjected to short-term creep tests in the study. T92 steel tubes were normalized at either 1213 K (L) or 1333 K (H) for 1 h, followed by tempering (T) at 1033 K for 2 h. After the normalizing and tempering treatments, the HT samples comprised finer precipitates but in greater numbers along the prior austenite grain boundaries (PAGBs) and martensite lath boundaries, as compared with those of the LT samples. The HAZ microstructures in the T92 steel welds were simulated by using an infrared heating system, which included over-tempering (OT, below A_{C1}) and partial transformation (PT, slightly below A_{C3}) zones. Martensite laths in the OT sample were more likely to be replaced by numerous cellular structures or subgrains together with spheroidized carbides mainly located at the lath and austenite grain boundaries. Furthermore, coarser but fewer carbides were found along the refined lath and grain boundaries in the PT samples, in comparison with other samples in each group. Short-term creep tests showed that the PT samples were more likely to fracture than other samples in each group. Moreover, under the same testing conditions, the microstructures of T92 steel were more stable and resistant to degradation than those of T91 steel after welding or loading at elevated temperatures. Such events were responsible for higher creep resistance of the simulated T92 samples than that of the simulated T91 samples under the same creep-rupture conditions.

Keywords: T92; thermal simulation; heat-affected zone; creep

1. Introduction

Boilers in steam power plants are often constructed using 9-12 Cr creep-resistant steels [1]. The extensive usage of ultra-supercritical (USC) fossil-fired power plants pushes the development of advanced ferritic steels, because such plants require improved creep-rupture strength and steam-oxidation resistance at 923 K. T92 steel (9Cr-0.5Mo-1.8W-VNbBN), which has good weldability [2], is one of the potential alloys applied in USC boilers [3]. The creep life of 9Cr ferritic steels can be improved by adding boron (B) to the alloys, which is associated with stabilized $M_{23}C_6$ carbides at the grain boundaries [4,5]. The addition of B can also decrease the hardness difference between distinct regions in modified 9Cr-1Mo steel welds [6]. Moreover, soluble B is responsible for repressing type

IV cracking of 9Cr-B welds [7]. The prominent high tensile strength of tungsten-added 9Cr steels at elevated temperature is attributed to the stabilized $M_2(CN)$ and $M_{23}C_6$ carbides and the decreased self-diffusivity of Fe [8]. Fine precipitates in 9-12 Cr steels can stabilize the subgrain structure of tempered martensite and lead to reduce creep rate [9]. Moreover, the coarsening rate of martensite laths in tempered 9Cr-W steels decreases with increasing tungsten content [10]. It is reported that the substitution of W for Mo effectively improves the creep resistance of the heat-affected zone (HAZ) in 9Cr steel welds [11].

The resistance to creep failure in the HAZ of a creep-resistant steel is an important factor in the construction of USC boilers. Creep cracking occurs in the HAZs of 9-12 Cr steel welds after long-term service at high temperature, which is known as type IV cracking [12–20]. The accumulation of voids in a crept Gr.91 steel weld over a long period contributes to type IV cracking [12]. After welding, complex phase transformation can occur within the narrow HAZ of the 9-12 Cr steel welds [21,22]. It has been reported that type IV cracking of creep-resistant steels may occur either in the intercritical heat-affected zone (ICHAZ) [13–16], which has experienced a peak temperature between A_{C1} and A_{C3} , or in the fine-grained heat-affected zone (FGHAZ) [17–20], which has been heated slightly above the A_{C3} temperature. The ICHAZ is also called the partial transformation zone (PTZ), in which partial transformation or incomplete austenite formation occurs during the heating cycle of welding [23]. Heating at around the A_{C1} of Gr.91 steel may induce short-time over-tempering, resulting in the recovery of dislocations, breakdown of the lath structure, polygonization, and carbide spheroidizing and coarsening [24]. In addition, the creep-rupture lives of advanced creep-resistant steel welds can be improved by using electron-beam welding to reduce the HAZ width [25,26]. The tensile strength [27] and creep-rupture life [6] of P91 steel increase with an increase in the normalizing temperature. Increasing the normalizing temperature also improves the strength of the ICHAZ [14] and prolongs the creep-rupture life of Gr.91 steel [28,29]. It is reported that ausforming T/P91 steel can obviously increase the amount of MX precipitates and improve the creep strength of the steel [30]. However, in the 9Cr steel after long-term aging at elevated temperatures, the lath structure is degraded and coarse Laves and Z phases are formed [31,32].

T92 steel tubes have been widely used in advanced supercritical boilers to replace Gr.91 tubes. As reported in prior works, the simulated HAZ microstructures of Gr.91 steel are sensitive to thermal cycles [24,29]. Moreover, normalizing Gr.91 steel at higher temperature is beneficial to improving its creep resistance [29]. To date, the microstructural evolutions and short-term creep tests of simulated HAZs present in a T92 steel weld have not been studied extensively. Moreover, the reasons for the superior creep properties of a T92 steel weld relative those of a Gr.91 one have not been clearly determined. In this study, as-received T92 steel tubes were normalized at either 1213 K or 1333 K for 1 h and tempered at 1033 K for 2 h. The effects of the normalizing treatments and thermal simulations on the HAZ microstructures and creep resistance of T92 steel were evaluated. Constant load tests were achieved to determine the short-term creep life of the simulated samples, and the results were compared with those of the base substrates. The intricate microstructures of the samples were inspected by transmission electron microscopy (TEM). The grain sizes and grain boundary characteristics of distinct samples were analyzed by electron backscatter diffraction (EBSD).

2. Materials and Experimental Procedures

T92 steel tubes 2 inches in diameter with a wall thickness of 3/8 inch were used in this study. The chemical composition in wt % of the T92 steel was 8.89 Cr, 0.47 Mo, 1.76 W, 0.003 B, 0.12 C, 0.43 Mn, 0.23 Si, 0.014 P, 0.002 S, 0.24 Ni, 0.20 V, 0.05 Nb, 0.038 N, 0.003 Ti, and the balance Fe. The as-received steel tubes were normalized at either 1213 K (L) or 1333 K (H) for 1 h in high vacuum, followed by Ar-assisted cooling to room temperature and then tempering at 1033 K for 2 h. The normalized and tempered substrates were named LT or HT samples according to the normalizing temperature. The A_{C1} , A_{C3} , M_s , and M_f temperatures were measured by a DIL 805A/D dilatometer (TA Instruments, Hüllhorst, Germany) at heating and cooling rates of 15 K/sec [33]. The A_{C1} , A_{C3} , M_s , and M_f temperatures

were 1159, 1207, 663, and 497 K, respectively. The HAZ microstructures in the T92 welds were simulated by using an infrared heating system, heating the LT and HT substrates to 1133 or 1173 K for 1 min, which was either slightly below the A_{C1} temperature (over-tempered, OT) or a little below the A_{C3} temperature (partial transformation, PT). After infrared heating, the simulated specimens were tempered at 1033 K for 2 h to meet the requirement of post-weld heat treatment of a T92 weld. It has been reported that short-time annealing at 750 °C can be applied to thin-walled T91 steel welds [34]. Regarding the thermally simulated samples, and for the LT-OT sample, the LT sample, which was previously normalized at 1213 K and then tempered at 1033 K, was heated to 1133 K for 1 min by infrared heating, followed by tempering at 1033 K for 2 h. For the HT-PT sample, the HT sample was heated to 1173 K for 1 min and then tempered at 1033 K for 2 h.

An MVK-G1500 Vickers hardness tester (Mitutoyo, Kawasaki, Japan) was used to measure the specimen hardness at an applied load of 300 g for 15 sec. The shown sample hardnesses were the averages of repeated measurements. To investigate the effects of the welding thermal cycles on the creep resistance of the simulated specimens at elevated temperature, the simulated tempered specimens were loaded with dead weight under one of two conditions—the 903 K/120 MPa or 933 K/80 MPa. The samples for creep tests [24,29] were cut from the steel tube by an electro-discharged wire cutter. The microstructures of various specimens were inspected with a BX51 optical microscope (OM, Olympus, Tokyo, Japan) and a JSM-7100F scanning electron microscope (SEM, JEOL, Tokyo, Japan). The fractured zones for further inspection were cut by a low-speed diamond saw and hot mounted in an epoxy; subsequently, standard metallographic preparations were performed. The details of the microstructures of the specimens were observed with a JEM-2000EX TEM (JEOL, Tokyo, Japan). Thin foils were prepared by twin-jet polishing in an electrolyte consisting of 75% ethanol, 20% $C_3H_5(OH)_3$ and 5% $HClO_4$ acid at -20 °C. Moreover, the specimens were also examined with an SEM equipped with a NordlysMax² EBSD detector (Oxford Instruments, Abingdon, UK) to reveal the grain size and the high-angle and subgrain boundaries of the specimens.

3. Results

Each T92 tube was normalized at either 1213 K (L) or 1333 K (H) for 1 h and tempered at 1033 K for 2 h (T). Under the as-normalized condition, the hardnesses of the L and H specimens were HV 407 and HV 389, respectively. The lower normalizing temperature resulted in a slightly higher hardness as confirmed by multiple tests. After tempering at 1033 K for 2 h, the LT and HT specimens had nearly the same hardness of HV 245. Under the same normalized and tempered conditions, the hardness of the Gr.91 steel was about HV 20 lower than that of the T92 steel [29,33]. Under the simulated over-tempered condition, the LT-OT and HT-OT specimens showed minor decreases in hardness to HV 206, regardless of the prior normalizing condition. In the specimens heated to below the A_{C3} temperature, the hardness of the HT-PT specimen (HV 220) was slightly higher than that of the LT-PT one (HV 210). As compared with those of the LT and HT specimens, the decreases in hardness of all the simulated specimens were related to the degraded microstructures of the specimens, as is shown below. It was obvious that the thermal cycles during welding would cause microstructural degradation, which accounted for the decline in the mechanical properties of the T92 steel weld.

Figure 1 presents SEM micrographs showing the typical microstructures of various specimens after tempering at 1033 K for 2 h. As shown in Figure 1a,b, the normalized and tempered microstructures of the LT and HT specimens comprised lath martensite packets with lath and austenite boundaries decorated by $M_{23}C_6$ carbides. The prior austenite grain sizes (PAGSs) of the specimens were determined by means of the line-intercept method and further confirmed by EBSD maps, as described in the following section. The PAGSs of the LT and HT specimens were about 8 and 26 μm , respectively. It was found that the lath boundaries of the HT sample were more densely decorated with precipitates (Figure 1b) than were those of the LT sample (Figure 1a). It has been reported that increasing the normalizing temperature from 1323 K to 1423 K also causes a decrease in the $M_{23}C_6$ carbide size, which is associated with an increase in the tensile strength but a reduction in the ductility of P91 steel [6].

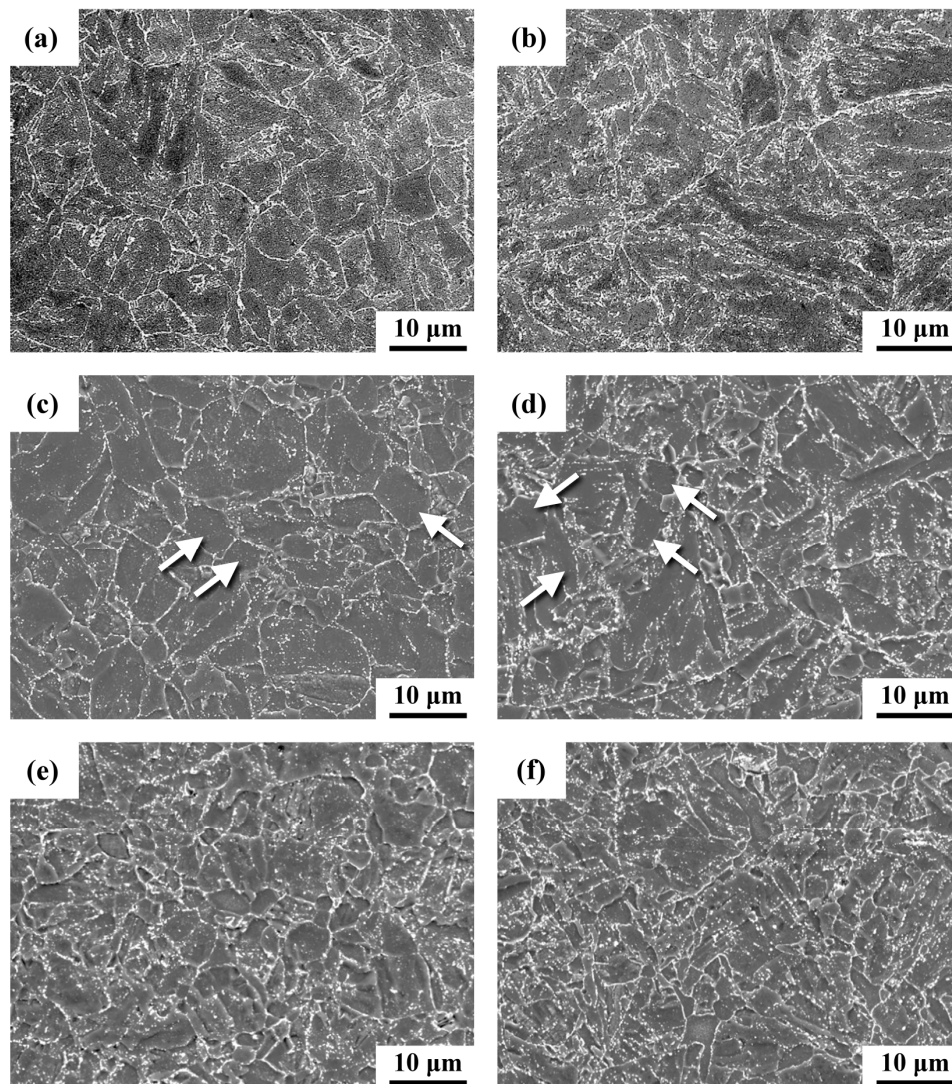


Figure 1. SEM micrographs of the (a) LT, (b) HT, (c) LT-OT, (d) HT-OT, (e) LT-PT, and (f) HT-PT samples.

In the over-tempered (OT) specimens, a decrease in the carbide density and an increase in the carbide size were observed (Figure 1c,d). In addition, the lath morphologies of the LT-OT and HT-OT specimens were not as prominent as those of the LT and HT specimens. It was noticed that the precipitates in the OT specimens were distributed less uniformly than those in the counterpart substrates. Another interesting finding was the presence of fine grains in the LT-OT and HT-OT samples. Some patches (indicated by arrows) in the OT specimens comprised few precipitates and displayed a vague lath morphology, possibly due to the over-tempering. Newly formed fine grains were more likely to be observed in both PT specimens, as shown in Figure 1e,f. Uneven grain sizes were also observed in the HT-PT sample (Figure 1f). In previous works [23,24], the as-welded ICHAZ (or partial transformation zone) consisted of fine ferrite subgrains and fresh fine martensite, which were responsible for a refined granular structure. The coalescence of carbide-free lath martensite in the normalized and tempered specimen during the heating cycle leads to the formation of ferrite subgrains in the PT specimen [23].

Inverse pole figures (IPFs) showing the individual grain orientation in different colors in the investigated samples are displayed in Figure 2. An obvious change in color represents a large difference in grain orientation. In individual grains, martensite packets oriented in nearly the same direction are of the same color, whereas distinct color zones are related to the lath packets of different orientations. The PAGs and martensite packets of the HT specimen (Figure 2b) were obviously larger and coarser

than those of the LT specimen (Figure 2a). The martensite packets in the HT sample were also easier to distinguish than were those in the LT sample. In addition, the PAGSs of the LT and HT specimens were confirmed by IPFs, as they were similar in size to those measured by the line-intercept method.

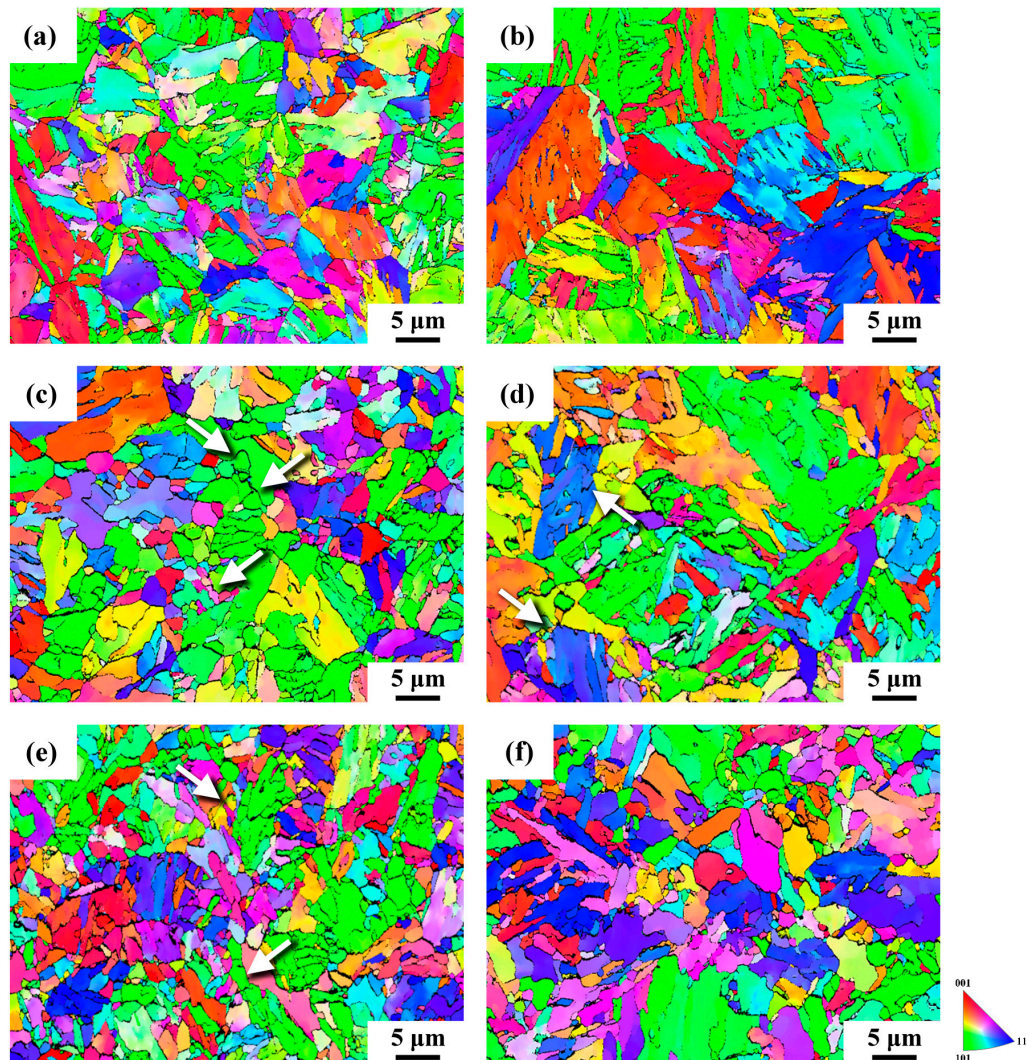


Figure 2. Inverse pole figures (IPFs) of the (a) LT, (b) HT, (c) LT-OT, (d) HT-OT, (e) LT-PT, and (f) HT-PT samples.

Figure 2c,d presents the IPFs of the LT-OT and HT-OT specimens. The lath structures in the LT-OT and HT-OT specimens were not as prominent as those in the LT and HT specimens. In fact, some elongated lath structures in the LT-OT and HT-OT specimens were divided into fine subgrains, as indicated by the arrows in Figure 2c,d. Those subgrains of the same color in the OT specimens should be aligned in nearly the same orientation. Therefore, it was deduced that those subgrains originally belonged to the same laths. Furthermore, the coarse lath structure present in the HT specimen was less prominent in the HT-OT specimen. The results implied that the short-time over-tempering assisted the recovery of excess dislocations and enhanced the polygonization process in the HAZ of the T92 weld. The degradation of the lath structure and the polygonization in the OT specimens were responsible for their lower hardness (HV 206) than that of the normalized and tempered specimens (HV 245).

The IPFs of the LT-PT and HT-PT samples are shown in Figure 2e,f. Numerous fine grains were more easily visible in the LT-PT sample (Figure 2e) than in the HT-PT sample (Figure 2f). Some elongated packets decomposed into several fine subgrains (indicated by the arrows) in the LT-PT specimen. Overall, the HT-PT specimen (Figure 2f) still retained traces of coarse martensite packets

and grain sizes, possibly due to the short-time thermal treatment. However, some very fine grains were located at the prior austenite grain boundaries (PAGBs). Those newly nucleated grains were the result of heating the Cr-Mo steels in the two-phase region.

Grain boundary maps showing the details of the austenite grain boundaries and sub-boundaries of various samples are displayed in Figure 3. It has been reported that the low-angle boundaries (subgrains), including the lath and block/packet boundaries within the matrix, have misorientations of $2\text{--}15^\circ$ and $50\text{--}60^\circ$, as classified by measuring the misorientation between adjacent grains. Prior austenite grain boundaries are identified as high-angle grain boundaries with misorientations of $15\text{--}50^\circ$. In this work, the low-angle grain boundaries are indicated by red ($1\text{--}5^\circ$) and green ($5\text{--}15^\circ$) lines, whereas high-angle grain boundaries ($15\text{--}62.5^\circ$) are indicated by blue. The grain boundary characteristics of the LT and HT specimens are shown in Figure 3a,b. It was obvious that the greater number of high-angle grain boundaries (blue) in the LT specimen (Figure 3a) accounted for its finer grain size than that of the HT specimen (Figure 3b). The larger grains in the HT specimen were more likely to have coarse martensite packets aligned in the same direction than were those in the LT specimen.

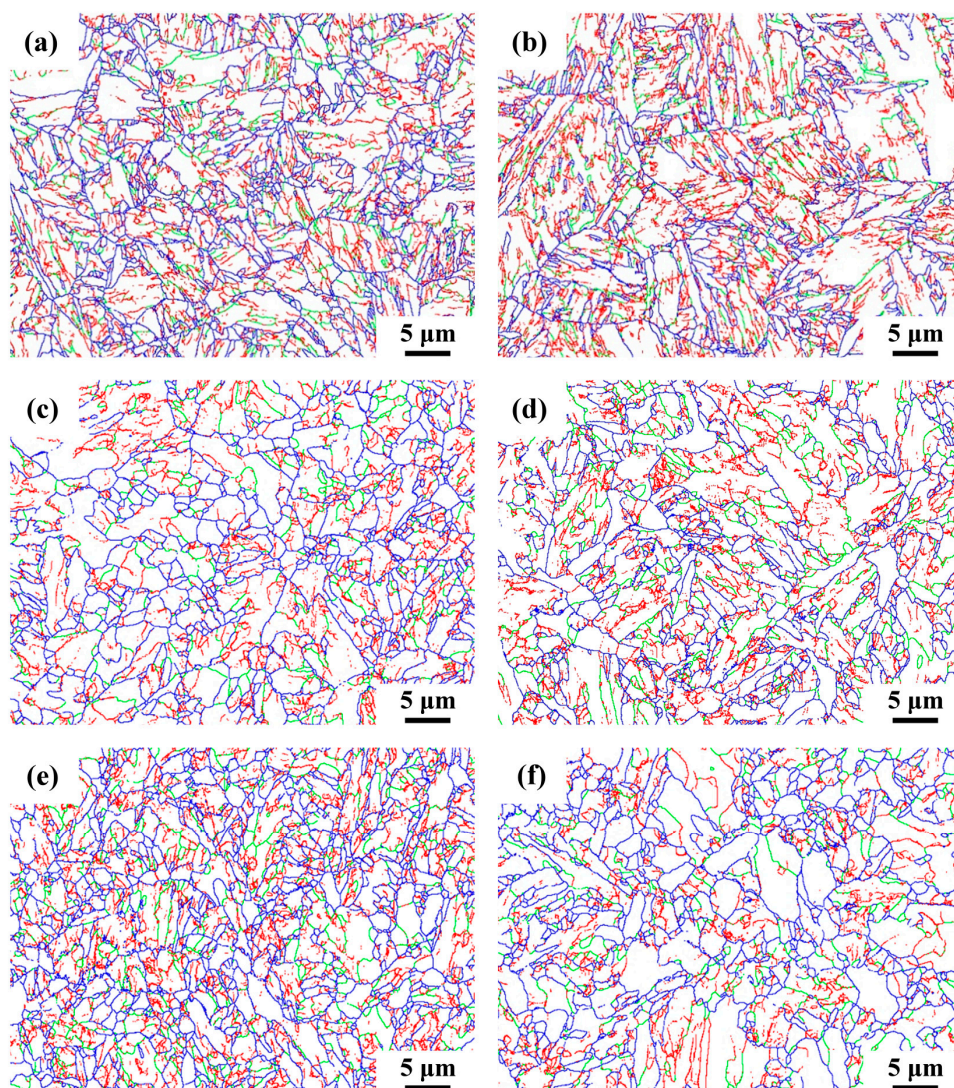


Figure 3. Grain boundary maps of the (a) LT, (b) HT, (c) LT-OT, (d) HT-OT, (e) LT-PT, and (f) HT-PT samples: $1\text{--}5^\circ$, $5\text{--}15^\circ$, $15\text{--}62.5^\circ$.

Figure 3c,d represents the grain boundary maps of the LT-OT and HT-OT samples. After the short-time over-tempering, the reduction in the amount of low-angle grain boundaries (red and green) in the OT sample indicated the obvious annihilation of dislocation densities in the tempered martensite, as compared with the LT and HT samples. In addition, many fine grains nucleated in the LT-OT and HT-OT specimens; those fine grains were associated with the polygonization after infrared heating and tempering. Additionally, those fine grains were more likely to comprise a few subgrain boundaries inside them. As shown in Figure 2c,d, those subgrains often had similar orientations (the same color), which were possibly related to the coalescence of lath martensite. It was deduced that the recovery of excess dislocations in the lath martensite enhanced the formation of subgrains with low dislocation densities in both OT specimens. Overall, the number of high-angle grain boundaries in the LT-OT specimen was higher than that in the HT-OT specimen.

In the samples heated below the A_{C3} temperature, the grains profiled by the high-angle grain boundaries of the LT-PT sample (Figure 3e) were finer and more irregular than those in other samples. Some extremely fine grains were found to nucleate along the PAGBs. Like the LT-PT sample, the HT-PT sample (Figure 3f) also comprised some unevenly sized grains with a few low-angle grain boundaries (white zones in the figure). Moreover, the grain boundary map of the HT-PT sample revealed that short-time thermal treatment did not completely refine the grain size; some coarse lath morphology was still present in the specimen (Figure 3f). In contrast, the partial transformation zone of Gr.91 steel revealed complete refinement after the same sample preparation [29]. The results also indicated that the white zones in the HT-PT specimen were generally larger than in the LT-PT one. The combination of the fine grain size and ferrite subgrains (white zones) in the PT specimens deteriorated their creep resistance relative to that of the normalized and tempered substrate.

Figure 4 presents TEM micrographs of T92 steel under different heat-treated conditions. In the normalized state, complete lath martensite with a high dislocation density was observed in the L sample (Figure 4a), which implied that the A_{C3} temperature of T92 steel was lower than 1213 K. Furthermore, no Cr-rich carbides were observed in the matrix or in the prior austenite grain boundaries (PAGBs) of the sample normalized at 1213 K. The lower normalizing temperature enhanced the formation of finer lath martensite within finer austenite grains. After tempering at 1033 K for 2 h, the details of the microstructures of the LT and HT samples are shown in Figure 4b,c. Under the normalized and tempered condition, the samples consisted of lath martensite packets with lath and austenite boundaries decorated by precipitates. During tempering, the number of dislocation densities decreased and that of carbide precipitates increased. The predominant precipitates that formed in the specimens were $M_{23}C_6$ carbides, as previously pointed out in other studies [19,35,36]. Non-uniform carbide distributions were observed in the tempered martensite; some lath packages had no precipitates dispersed along the lath boundaries. It is reported that increasing the normalizing temperature from 1323 K (1050 °C) to 1423 K (1150 °C) reduces the size of the $M_{23}C_6$ carbides in P91 steel [6]. Moreover, the width of the martensite laths and the size of the carbides increase with increasing tempering temperature [35]. In this work, the carbides in the HT sample were obviously smaller than those in the LT sample, and their distribution was more uniform. However, the lath width and packet size of the martensite in the HT specimen were wider and larger than those in the LT specimen.

Figure 5 shows the details of the microstructures of the simulated specimens of T92 steel. The recovery and carbide-coarsening of Gr.91 [16] and T92 [36] steels after short-time over-tempering accounted for the decrease in hardness of the OT specimen, relative to those of normalized and tempered substrates [16,23,36]. As shown in Figure 3c, fine white patches indicated lack of low-angle grain boundaries. The results indicated that the martensite laths in the LT-OT sample were more likely to be replaced by numerous cell structures or subgrains (Figure 5a). It seemed that spheroidized carbides were mainly located at the prior lath boundaries and/or PAGBs (Figure 5a). It was noticed that short-time over-tempering also facilitated the migration of lath boundaries, as indicated by the arrows. The presence of arrayed precipitates inside the grain accounted for the evidence of grain boundary migration. The presence of coarse carbides and ferrite subgrains in the LT-OT sample degraded its

creep resistance relative to that of the LT sample. The HT-OT sample had microstructures similar to those observed in the LT-OT sample (Figure 5b). As a whole, the carbides in the HT-OT sample were similar in size to those in the LT-OT sample, but greater in number. Such results could be attributed to the inherent carbide characteristics of the substrates.

The coexistence of refined fresh martensite with a high dislocation density and carbide-free ferrite subgrains caused incomplete hardening of the as-simulated PT or ICHAZ specimens [23,37]. It has been pointed out that fine lath martensite with undissolved $M_{23}C_6$ and MX particles, along with Cr-rich ferrite, are formed in the FGHAZ of a modified 9Cr-1Mo steel weld heated to temperatures between A_{C1} and A_{C3} . [23,34,38]. Under the as-simulated condition, most $M_{23}C_6$ carbides heated to slightly below the A_{C3} temperature dissolve into the matrix, and few residual carbides remain [23,24]. After tempering, carbides precipitated mainly at the lath boundaries and in ferrite subgrains. As shown in Figure 5c, the lath boundaries of the LT-PT specimen were decorated by very coarse precipitates. It was deduced that those coarse carbides in the LT-PT specimen were likely associated with the growth of residual carbides during tempering. The carbides in the HT-PT sample were larger than those in the HT-OT and HT samples. Inevitably, the thermal cycles imposed by welding caused the microstructures to deteriorate and degraded the creep resistance of the T92 steel weld.

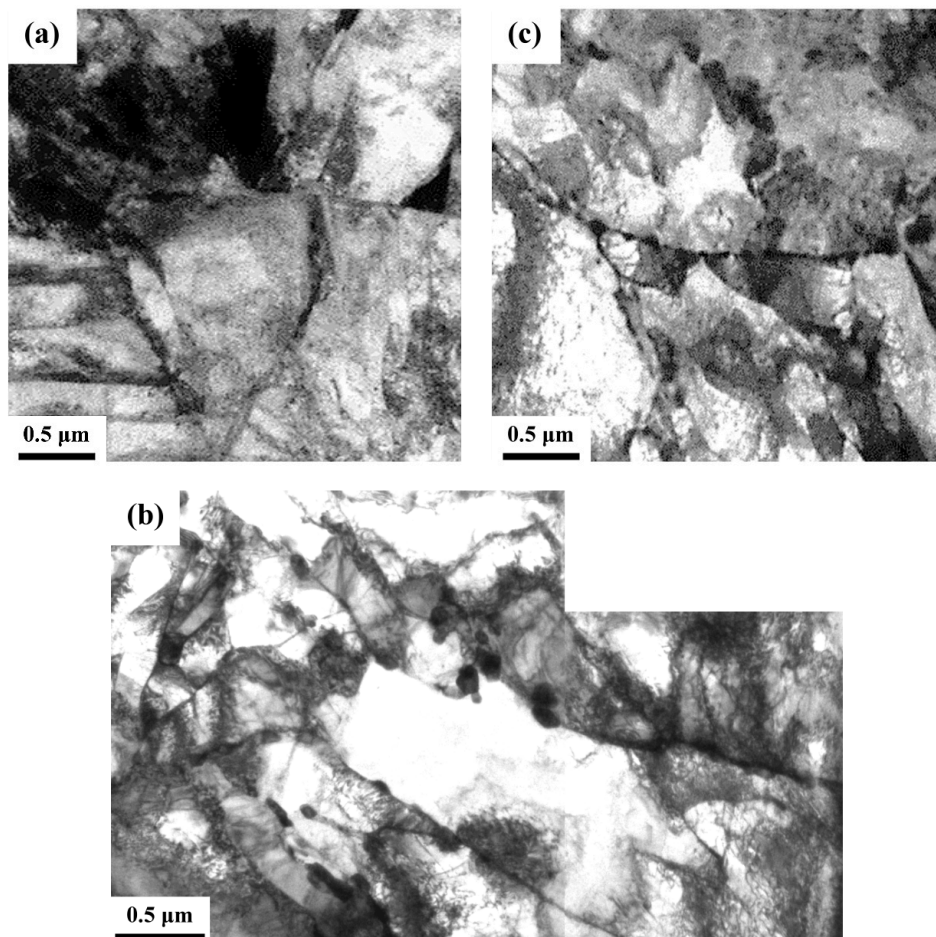


Figure 4. Transmission electron microscopy (TEM) micrographs of the (a) L, (b) LT, and (c) HT samples.

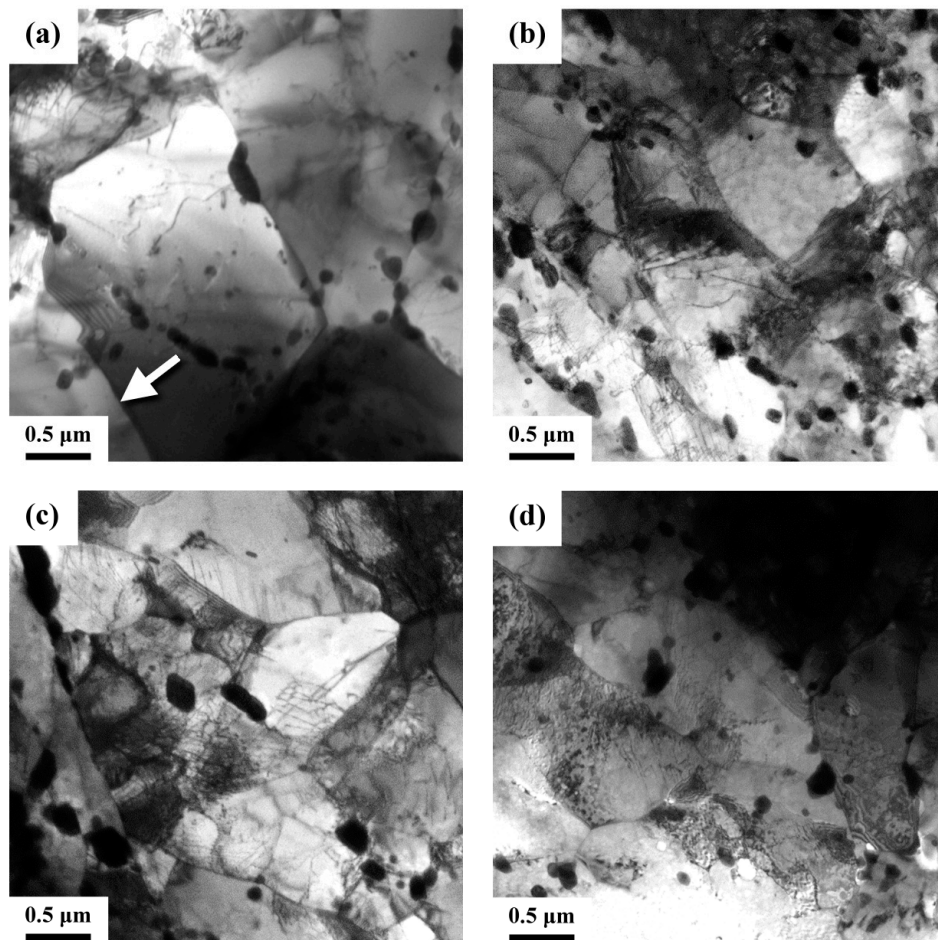


Figure 5. TEM micrographs of the (a) LT-OT, (b) HT-OT, (c) LT-PT, and (d) HT-PT samples.

Figure 6 shows the results of short-term creep tests of the specimens loaded under one of two conditions—903 K/120 MPa or 933 K/80 MPa. In each group, three tests were performed on each specific type of sample under a given creep condition. It should be noted that the conducted creep tests are short in duration and do not always reflect the nature of long-term work. The stress-rupture tests were terminated if the tested specimens did not rupture after 4000 h of straining. The specimen elongation was also measured as an index of the creep strength of the specimens at elevated temperature. Moreover, the results of the short-term creep tests of simulated Gr.91 samples [29] were included in Figure 6 to compare with the data of T92 samples. As shown in Figure 6, the LT and HT samples were resistant to creep failure and did not fracture within the testing period, regardless of testing condition. The stress-rupture lives of the simulated samples were shortened, especially those of the PT samples. Under the 903 K/120 MPa condition (Figure 6a), the PT samples were more likely to rupture in each group, particularly the LT-PT sample. Under the creep condition of 933 K/80 MPa, only the LT-PT and HT-PT samples fractured within the testing period. The results also indicated that the fractured samples were associated with measurable rupture elongations (Figure 6b,d). As shown in Figure 6c, only the LT-PT and HT-PT samples fractured within the creep-testing period. It was noticed that the creep life of the HT-PT sample was shorter than that of the LT-PT one (Figure 6c); however, the reasons remained undetermined. It was obvious that the thermal cycles of welding, especially in those sites heated to below the A_{C3} temperature, had an obviously adverse effect on the creep resistance of the T92 steel weld.

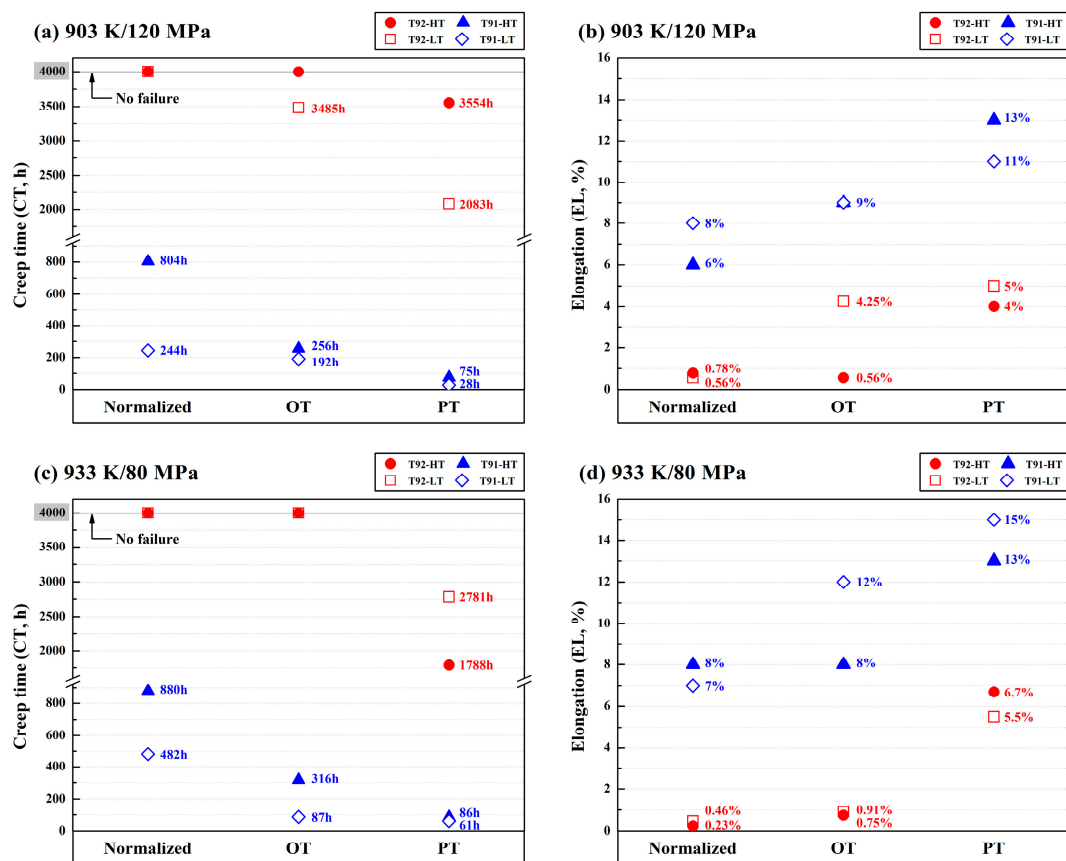


Figure 6. Creep time and elongation of distinct samples after short-term creep test strained at (a,b) 903 K/120 MPa and (c,d) 933 K/80 MPa.

As shown in Figure 6b,d, the fractured samples exhibited low ductility, whereas the unfractured ones showed no change in sample length. The typical fractured surface features and microstructures near the fracture zones of creep-ruptured samples are shown in Figure 7. For microstructural observations, the ruptured samples were cut and subjected to metallographic preparations for further SEM examinations in backscattered-electron (BSE) image. Regardless of the testing condition, the fracture surfaces of all the creep-ruptured samples consisted of predominantly dimple fracture mixed with a little intergranular separation (Figure 7a). Under the testing condition of 903 K/120 MPa, the LT-OT and LT-PT samples displayed similar microstructures near the fracture zone, that is, a refined granular structure with coarse precipitates decorating the grain boundaries (Figure 7b). The original lath features present in the samples were barely visible in the fracture zone (Figure 7b). Moreover, the HT-PT sample had mixed grain sizes with coarse precipitates at the grain boundaries (Figure 7c). It was noticed that the initiation and propagation of the crept microcracks were associated with high-angle grain boundary separations. Moreover, the vague trace of a coarse martensite package in the HT-PT sample could still be seen. Such microstructural characteristics confirmed that the HT-PT sample was more resistant to creep failure than was the LT-PT sample. However, a great change in microstructural features occurred in the HT-PT sample strained under the 933 K/80 MPa condition. Fine grains with coarse precipitates dispersed intra- and intergranularly were present near the fracture zone of the crept HT-PT samples (Figure 7d). It was deduced that dynamic recrystallization of the HT-PT sample, which occurred under straining at 933 K, accounted for the obvious decay of its creep resistance. However, the exact mechanism of such great change has yet to be determined.

The IPF maps around the fracture zones of the creep-ruptured samples are displayed in Figure 8. Under the 903 K/120 MPa condition, the LT-OT and LT-PT samples exhibited fine-grained structures and textures (Figure 8a,b), particularly the LT-PT sample. By contrast, the HT-PT sample still possessed

coarse grains with lath structures inside them (Figure 8c). Under the 933 K/80 MPa testing condition, dynamic recrystallization resulted in the formation of refined grains in the HT-PT sample (Figure 8d), that is, the original coarse grains in the uncrept sample were replaced by fine grains around the fracture zone of the crept sample. Moreover, the LT-PT samples tested under the 903 K/120 MPa and 933 K/80 MPa (not shown here) conditions revealed similar morphologies. Thus, the formation of refined substructures during straining of the HT-PT sample at 933 K partly accounted for the lowered stress-rupture life, as compared with those strained at 903 K.

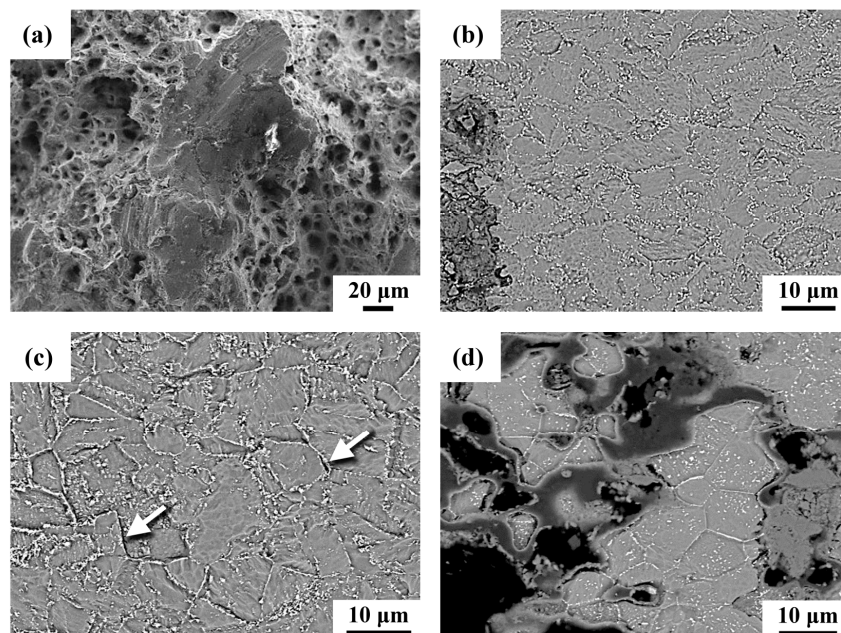


Figure 7. SEM micrographs of (a) fracture surface appearance of the HT-PT sample; microstructure near the fracture zone of the (b) LT-OT, (c) HT-PT samples tested at 903 K/120 MPa, (d) HT-PT samples tested at 933 K/80 MPa.

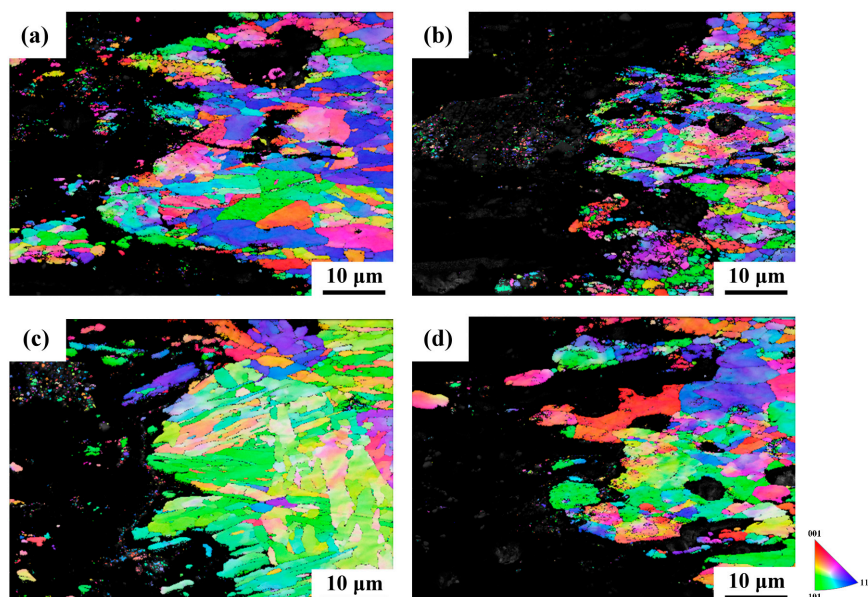


Figure 8. IPF maps of the fracture zones of the (a) LT-OT, (b) LT-PT, and (c) HT-PT samples tested at 903 K/120 MPa; (d) HT-PT sample tested at 933 K/80 MPa.

4. Discussion

Increasing the normalizing temperature from 1213 K to 1333 K caused an increase in the martensite packet sizes and the PAGSs of the T92 steel. The measured PAGSs of the LT and HT samples were about 8 and 26 μm , respectively. TEM micrographs displayed that the carbides in the tempered T92 steel were finer and that the carbide distribution was more uniform when the normalizing temperature was higher. Dislocation recovery, polygonization, and carbide-coarsening occurred in the over-tempered (OT) samples, resulting in a decline in hardness relative to those of the LT and HT samples. Moreover, the grain boundary maps showed that the white zones without low-angle grain boundaries in the OT samples were associated with the formation of ferrite subgrains. Overall, the white zones in the LT-OT sample were smaller than those in the HT-OT one, possibly due to the combination of fine laths into ferrite subgrains during subsequent infrared heating and tempering.

The tempered intercritical (IC) or partial transformation (PT) HAZ, which was heated to below the A_{C3} temperature, exhibited refined grain sizes, as shown in Figure 3e,f. The microstructures of the PT samples comprised mainly ferrite subgrains, tempered martensite, and very coarse carbides, as shown in Figure 5. Therefore, the mixed microstructures in the PT samples also exhibited a fine-grained structure. Moreover, the presence of excessively coarse carbides and ferrite subgrains was expected to lower the creep resistance of the LT-PT and HT-PT samples. It is reported that the number of cavities, which form mainly along the grain boundaries of the FGHAZ, is much higher than those in other zones of Gr.91 steel welds [39]. Moreover, the finer PAGS in the FGHAZ leads to a higher recovery rate of excess dislocations, which results in higher rates of subgrain growth and precipitate coarsening [40]. Regardless of the testing condition, the PT sample had lower creep resistance than the other samples in each group did, which was consistent with other published works.

It has been reported that increasing the normalizing temperature can improve the creep resistance of Gr.91 steel [6,29]. In this study, increasing the normalizing temperature of T92 steel enhanced the formation of finer but greater amounts of carbides after tempering. As shown in Figure 6a, for the samples strained under the 903 K/120 MPa condition, the creep resistance of the HT-PT sample was higher than that of the LT-PT one. In addition, the HT-OT sample was resistant to fracture, but the LT-OT sample ruptured within the testing period. Under the 903 K/120 MPa condition, the IPF map of the crept fracture zone of an HT-PT sample showed a retained coarse lath structure (Figure 8c), which implied that the microstructural degradation was not as severe in this sample as in the samples with extensive recrystallization. However, under the 933 K/80 MPa condition, the creep life of the HT-PT sample was shorter than that of the LT-PT sample (Figure 6c). Moreover, the IPF map of the crept fracture zone of an HT-PT sample strained under the 933 K/80 MPa condition displayed a complete fine-grained structure (Figure 8d). The exact reasons why the creep life of the HT-PT sample was shorter than that of the LT-PT sample are not known at this time. It was noticed that the white zones in the HT-PT sample could be rather large relative to those in other samples (Figure 3f). In the HT-PT sample strained under the 933 K/80 MPa condition, the presence of coarse ferrite and the occurrence of rapidly dynamic recrystallization resulted in significant softening; thus, the HT-PT sample had poor creep resistance. Simulated Gr.91 samples with degraded microstructures confirmed that this alloy is sensitive to the imposed thermal cycles during welding [24,29]. Coarse ferrite subgrains are responsible mainly for the lower creep resistance of PT samples [29]. In addition, complete grain refinement in the simulated Gr.91 samples is more likely to be obtained even for the samples normalized at higher temperature [29]. Rapid coalescence of lath structure and dynamic recrystallization occur during the short-term creep tests of Gr.91 samples, which are associated with their short creep lives. The results of this study indicated that the microstructures of the T92 steel were much more stable and resistant to change than those of the Gr.91 steel, if welding thermal cycles or loading at elevated temperature were applied. Such events were responsible for the much higher creep resistance of the T92 steel welds than that of the Gr.91 ones under the same testing conditions.

5. Conclusions

The microstructural evolutions of simulated HAZs of T92 steel tube normalized at different temperatures were investigated, and short-term creep tests were performed. The superior creep properties of the simulated microstructures in the HAZ of a T92 steel weld relative to those of a Gr.91 one were also addressed. Important conclusions are listed below.

- (1) Increasing the normalizing temperature of T92 steel tube from 1213 K to 1333 K led to the formation of finer carbides but in greater numbers in the sample after tempering at 1033 K for 2 h.
- (2) Dislocation recovery, polygonization, and carbide-coarsening occurred in the over-tempered (OT) samples, leading to a decline in hardness relative to those of the normalized and tempered substrates. The formation of soft zones or ferrite subgrains in the OT samples played an important role in degrading their creep resistance, as compared with the LT and HT samples.
- (3) The PT samples, especially the LT-PT one, comprised fine-grained structures. All the creep cracks were found to nucleate mainly at the high-angle grain boundaries; thus, the fine-grained structure had an obviously adverse effect on its creep resistance. Coarse carbides along the grain and subgrain boundaries and the presence of ferrite soft zones accounted for the inferior creep resistance of the PT samples.
- (4) The microstructures of the T92 steel tube were more stable and resistant to degradation than those of the Gr.91 steel, if welding thermal cycles or loading at elevated temperatures were applied. Such events were responsible for the better creep resistance of the simulated T92 samples than that of the simulated Gr.91 ones under the same creep-rupture conditions.

Author Contributions: L.-W.T. planned and organized this study. R.-K.S. assisted with the EBSD and microstructural characteristics evaluation. T.-J.W., T.-C.C., and C.-C.L. shared duties in conducting all of the experiments. All authors were involved in completing the manuscript.

Funding: This research was funded by the Ministry of Science and Technology of the Republic of China, MOST 106-2221-E-019-060-MY3.

Conflicts of Interest: The authors declare no conflict of interest.

References

1. Viswanathan, R.; Bakker, W.T. Materials for boilers in ultra supercritical power plants. In Proceedings of the International Joint Power Generation Conference, Miami Beach, FL, USA, 23–26 July 2000.
2. Brózda, J. New generation creep-resistant steels, their weldability and properties of welded joints: T/P92 steel. *Weld. Int.* **2005**, *19*, 5–13. [[CrossRef](#)]
3. Caminada, S.; Cumino, G.; Lauro, A. Experiences in the use of advanced materials for Ultra Super Critical thermoelectric power plants: ASTM P92 grade and its weldability. *Weld. Int.* **2012**, *26*, 910–920. [[CrossRef](#)]
4. Horiuchi, T.; Igarashi, M.; Abe, F. Improved utilization of added B in 9Cr heat-resistant steels containing W. *ISIJ Int.* **2002**, *42*, S67–S71. [[CrossRef](#)]
5. Albert, S.K.; Kondo, M.; Tabuchi, M.; Yin, F.; Sawada, K.; Abe, F. Improving the creep properties of 9Cr-3W-3Co-NbV steels and their weld joints by the addition of boron. *Metall. Mater. Trans. A* **2005**, *36*, 333–343. [[CrossRef](#)]
6. Das, C.R.; Albert, S.K.; Swaminathan, J.; Raju, S.; Bhaduri, A.K.; Murty, B.S. Transition of crack from Type IV to Type II resulting from improved utilization of Boron in the modified 9Cr-1Mo steel weldment. *Metall. Mater. Trans. A* **2012**, *43*, 3724–3741. [[CrossRef](#)]
7. Abe, F.; Tabuchi, M.; Tsukamoto, S.; Shirane, T. Microstructure evolution in HAZ and suppression of Type IV fracture in advanced ferritic power plant steels. *Int. J. Press. Vessel. Pip.* **2010**, *87*, 598–604. [[CrossRef](#)]
8. Hong, S.G.; Lee, W.B.; Park, C.G. The effects of tungsten addition on the microstructural stability of 9Cr-Mo Steels. *J. Nucl. Mater.* **2001**, *288*, 202–207. [[CrossRef](#)]
9. Chilukuru, H.; Durst, K.; Wadekar, S.; Schwienheer, M.; Scholz, A.; Berger, C.; Mayer, K.H.; Blum, W. Coarsening of precipitates and degradation of creep resistance in tempered martensite steels. *Mater. Sci. Eng. A* **2009**, *510–511*, 81–87. [[CrossRef](#)]

10. Abe, F. Coarsening behavior of lath and its effect on creep rates in tempered martensitic 9Cr–W steels. *Mater. Sci. Eng. A* **2004**, *387*, 565–569. [[CrossRef](#)]
11. Ootoguro, Y.; Matsubara, M.; Itoh, I.; Nakazawa, T. Creep rupture strength of heat affected zone for 9Cr ferritic heat resisting steels. *Nucl. Eng. Des.* **2000**, *196*, 51–61. [[CrossRef](#)]
12. Li, Y.; Monma, Y.; Hongo, H.; Tabuchi, M. Evaluation of creep damage in a welded joint of modified 9Cr–1Mo steel. *J. Nucl. Mater.* **2010**, *405*, 44–49. [[CrossRef](#)]
13. Gaffard, V.; Gourgues-Lorenzon, A.F.; Besson, J. High temperature creep flow and damage properties of the weakest area of 9Cr1Mo–NbV martensitic steel weldments. *ISIJ Int.* **2005**, *45*, 1915–1924. [[CrossRef](#)]
14. Das, C.R.; Albert, S.K.; Bhaduri, A.K.; Srinivasan, G.; Murty, B.S. Effect of prior microstructure on microstructure and mechanical properties of modified 9Cr–1Mo steel weld joints. *Mater. Sci. Eng. A* **2008**, *477*, 185–192. [[CrossRef](#)]
15. Divya, M.; Das, C.R.; Albert, S.K.; Goyal, S.; Ganesh, P.; Kaul, R.; Swaminathan, J.; Murty, B.S.; Kukreja, L.M.; Bhaduri, A.K. Influence of welding process on Type IV cracking behavior of P91 steel. *Mater. Sci. Eng. A* **2014**, *613*, 148–158. [[CrossRef](#)]
16. Wang, Y.; Li, L.; Kannan, R. Transition from Type IV to Type I cracking in heat-treated grade 91 steel weldments. *Mater. Sci. Eng. A* **2018**, *714*, 1–13. [[CrossRef](#)]
17. Albert, S.K.; Matsui, M.; Watanabe, T.; Hongo, H.; Kubo, K.; Tabuchi, M. Variation in the Type IV cracking behaviour of a high Cr steel weld with post weld heat treatment. *Int. J. Press. Vessel. Pip.* **2003**, *80*, 405–413. [[CrossRef](#)]
18. Hongo, H.; Tabuchi, M.; Watanabe, T. Type IV creep damage behavior in Gr. 91 steel welded joints. *Metall. Mater. Trans. A* **2012**, *43*, 1163–1173. [[CrossRef](#)]
19. Xue, W.; Pan, Q.G.; Ren, Y.Y.; Shang, W.; Zeng, H.Q.; Liu, H. Microstructure and type IV cracking behavior of HAZ in P92 steel weldment. *Mater. Sci. Eng. A* **2012**, *552*, 493–501. [[CrossRef](#)]
20. Liu, Y.; Tsukamoto, S.; Shirane, T.; Abe, F. Formation mechanism of type IV failure in high Cr ferritic heat-resistant steel-welded joint. *Metall. Mater. Trans. A* **2013**, *44*, 4626–4633. [[CrossRef](#)]
21. Velkavrh, I.; Kafexhiu, F.; Klien, S.; Diem, A.; Podgornik, B. Tempering-Induced Microstructural Changes in the Weld Heat-Affected Zone of 9 to 12 Pct Cr Steels and Their Influence on Sliding Wear. *Metall. Mater. Trans. A* **2017**, *48*, 109–125. [[CrossRef](#)]
22. Milović, L.; Vuherer, T.; Blačić, I.; Vrhovac, M.; Stanković, M. Microstructures and mechanical properties of creep resistant steel for application at elevated temperatures. *Mater. Des.* **2013**, *46*, 660–667. [[CrossRef](#)]
23. Xu, X.; West, G.D.; Siefert, J.A.; Parker, J.D.; Thomson, R.C. The influence of thermal cycles on the microstructure of grade 92 steel. *Metall. Mater. Trans. A* **2017**, *48*, 5396–5414. [[CrossRef](#)]
24. Hsiao, T.H.; Chen, T.C.; Jeng, S.L.; Chung, T.J.; Tsay, L.W. Effects of simulated microstructure on the creep rupture of the modified 9Cr–1Mo steel. *J. Mater. Eng. Perform.* **2016**, *25*, 4317–4325. [[CrossRef](#)]
25. Tabuchi, M.; Watanabe, T.; Kubo, K.; Matsui, M.; Kinugawa, J.; Abe, F. Creep crack growth behavior in the HAZ of weldments of W containing high Cr steel. *Int. J. Press. Vessel. Pip.* **2001**, *78*, 779–784. [[CrossRef](#)]
26. Abe, F.; Tabuchi, M. Microstructure and creep strength of welds in advanced ferritic power plant steels. *Sci. Technol. Weld. Join.* **2004**, *9*, 22–30. [[CrossRef](#)]
27. Pandey, C.; Giri, A.; Mahapatra, M.M. Effect of normalizing temperature on microstructural stability and mechanical properties of creep strength enhanced ferritic P91 steel. *Mater. Sci. Eng. A* **2016**, *657*, 173–184. [[CrossRef](#)]
28. Totemeier, T.C.; Tian, H.; Simpson, J.A. Effect of normalization temperature on the creep strength of modified 9Cr–1Mo steel. *Metall. Mater. Trans. A* **2006**, *37*, 1519–1525. [[CrossRef](#)]
29. Wu, H.W.; Wu, T.J.; Shiue, R.K.; Tsay, L.W. The Effect of Normalizing Temperature on the Short-Term Creep Rupture of the Simulated HAZ in Gr. 91 Steel Welds. *Metals* **2018**, *8*, 1072. [[CrossRef](#)]
30. Vivas, J.; Capdevila, C.; Jimenez, J.A.; Benito-Alfonso, M.; San-Martin, D. Effect of Ausforming Temperature on the Microstructure of G91 Steel. *Metals* **2017**, *7*, 236. [[CrossRef](#)]
31. Zieliński, A.; Sroka, M.; Miczka, M.; Śliwa, A. Forecasting the particle diameter size distribution in P92 (X10CrWMoVNb9-2) steel after long-term ageing at 600 and 650 °C. *Arch. Metall. Mater.* **2016**, *61*, 753–760. [[CrossRef](#)]
32. Golański, G.; Zielińska-Lipiec, A.; Zieliński, A.; Sroka, M. Effect of long-term service on microstructure and mechanical properties of martensitic 9% Cr Steel. *J. Mater. Eng. Perform.* **2017**, *26*, 1101–1107. [[CrossRef](#)]

33. Peng, Y.Q.; Chen, T.C.; Chung, T.J.; Jeng, S.L.; Huang, R.T.; Tsay, L.W. Creep Rupture of the Simulated HAZ of T92 Steel Compared to that of a T91 Steel. *Materials* **2017**, *10*, 139. [[CrossRef](#)] [[PubMed](#)]
34. Wojsyk, K.; Golański, G.; Jasak, J.; Ślania, J.; Zieliński, A.; Urbańczyk, P. Influence of the annealing time after welding of the mechanical properties of welded joint of T91 steel. *Arch. Metall. Mater.* **2016**, *61*, 1425–1430. [[CrossRef](#)]
35. Zhao, D.; Zhang, S.; Zhang, H.; Li, S.; Xiao, H.; Wang, Y.; Wang, X. Effects of Tempering Temperature on the Microstructure and Mechanical Properties of T92 Heat-Resistant Steel. *Metals* **2019**, *9*, 194. [[CrossRef](#)]
36. Xu, X.; West, G.D.; Siefert, J.A.; Parker, J.D.; Thomson, R.C. Microstructure Characterization of the Heat Affected Zone in Grade 92 Steel Welds: Double-Pass and Multipass Welds. *Metall. Mater. Trans. A* **2018**, *49*, 1211–1230. [[CrossRef](#)]
37. Wang, Y.; Kannan, R.; Li, L. Correlation Between Intercritical Heat-Affected Zone and Type IV Creep Damage Zone in Gr. 91 Steel. *Metall. Mater. Trans. A* **2018**, *49*, 1264–1275. [[CrossRef](#)]
38. Sawada, K.; Hara, T.; Tabuchi, M.; Kimura, K.; Kubushiro, K. Microstructure Characterization of Heat Affected Zone After Welding in Mod.9Cr-1Mo Steel. *Mater. Charact.* **2015**, *101*, 106–113. [[CrossRef](#)]
39. Xu, J.A.; Zhong, X.Y.; Shoji, T.; Tatsuki, T.; Matsumura, Y.; Nakashima, M. Characterizations of the Microstructure of 9Cr-1Mo Steel Weld Joint After Long-Term Service in a Supercritical Fossil Power Plant. *Metall. Mater. Trans. A* **2018**, *49*, 4700–4709. [[CrossRef](#)]
40. Abd El-Azim, M.E.; Ibrahim, O.H.; El-Desoky, O.E. Long term creep behaviour of welded joints of P91 steel at 650 °C. *Mater. Sci. Eng. A* **2013**, *560*, 678–684. [[CrossRef](#)]



© 2019 by the authors. Licensee MDPI, Basel, Switzerland. This article is an open access article distributed under the terms and conditions of the Creative Commons Attribution (CC BY) license (<http://creativecommons.org/licenses/by/4.0/>).